Inorganic Chemistry

Article

pubs.acs.org/IC

Synthesis, Structure, and Magnetic Properties of Bithiophene- and Terthiophene-Linked Manganese Metal−Organic Frameworks

Lyndsey D. Earl, Brian O. Patrick, and Michael O. Wolf*

Department of Chemistry, University of British Columbia, Vancouver, British Columbia, V6T 1Z1 Canada

Supporting Information

ABSTRACT: A series of metal−organic frameworks (MOFs) containing manganese centers and oligothiophene dicarboxylate linkers have been synthesized: $[Mn(3PhT_2DC)(DMF)_{0.45}(H_2O)_{2.55}\cdot 1.55DMF]_n$ (**1**), $[Mn_6(3HT_2DC)_6(DMF)_3(H_2O)_5\cdot xDMF\cdot yH_2O]_n$ (**2**), $[Mn(T_3DC)(H_2O)_2]_n$ (**3**), $[Mn(T_3DC)(H_2O)_{1.5}]_n$ (**4**), and $[Mn(Ph_2T_3DC)(DMF)_2]_n$ (**5**) ($H_2$3PhT$_2$DC = 3,3′-diphenyl-2,2-bithiophene-5,5′-dicarboxylic acid; $H_2$3HT$_2$DC= 3,3′-dihexyl-2,2′-bithiophene-5,5′-dicarboxylic acid; H_2T_3DC = 2,2′:5′,2″-terthiophene-5,5″-dicarboxylic acid; $H_2Ph_2T_3DC$ = 3′,4′-diphenyl-2,2′:5′,2″-terthiophene-5,5″-dicarboxylic acid, DMF = *N*,*N*-dimethylformamide). Compound **1** exists as a 2D sheet, **2**−**4** are 3D frameworks, and **5** is a 1D chain. Compounds **3** and **4** are isomers, and **3**−**5** are the first examples of crystallographically characterized terthiophene coordination polymers. In the case of **1**, **2**, and **5**, the extended structure is sensitive to *β* substitution of the oligothiophene linkers. Compounds **1**−**3** and **5** show antiferromagnetic behavior with typical values of *g* and *J*, and **3** exhibits a spin canting transition at 40 K.

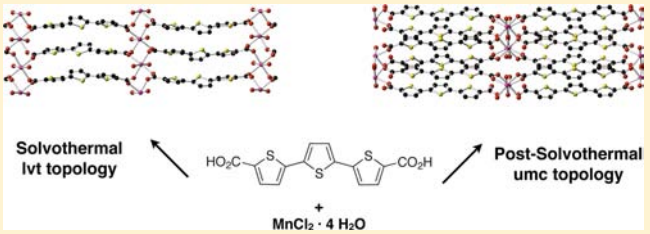

INTRODUCTION

The structural and electronic properties of longer chain oligothiophenes and polythiophenes are of significant interest for potential applications including light-emitting and photovoltaic devices, electrochromic materials, and chemical sensors.[1] Positional and orientational control of oligothiophenes is important for these potential applications, particularly for optimizing the efficiency of light-harvesting systems and controlling orientation-dependent charge transfer.[2] Functionalization of the *β* position of oligo- and polythiophenes with solubilizing and photoactive groups has proved to be a useful method for manipulating the physical and electronic structure of these materials.[3]

The synthesis and characterization of manganese coordination polymers containing oligothiophene linkers is of particular interest due to the local[4] and global[5] structural diversity, potential mixed valence character,[6] electronic activity,[7] and magnetic properties[8] of Mn^{2+} metal−organic frameworks (MOFs). Although Mn^{2+} is usually a high-spin d^5 metal center that quenches photoluminescence, the structural data obtained from these compounds will provide valuable information for engineering specific solid state interactions of oligothiophenes.

Methodical crystal engineering can be applied *via* incorporation of oligothiophene linkers into metal−organic frameworks to obtain orientational control of coordination polymers.[9] A myriad of MOFs containing thiophene-2,5-dicarboxylic acid have been reported,[10] though few oligothiophene metal−organic frameworks,[11−13] polyhedra,[14] or covalent-organic frameworks[15] have been synthesized. Examples of conjugated triaryl MOFs are limited to those containing *p*-terphenyl linkers.[16] Terthiophene coordination polymers have been synthesized[17] but not characterized crystallographically.

While examples of MOFs containing linkers with alkyl chains have been reported,[18] there have been few extensive studies looking into the influence of functional groups on the extended structure of coordination polymers. In this Article, we report how phenyl and *n*-hexyl substituents as well as thiophene oligomer length affect the coordination and extended structure within five new coordination polymers. The first examples of crystallographically characterized terthiophene coordination polymers are reported, including a set of isomers. In addition, the magnetic behavior of these new metal−organic frameworks and the correlation between magnetic susceptibility and structure are discussed.

EXPERIMENTAL SECTION

General Methods. $MnCl_2\cdot 4H_2O$ and *n*-butyllithium were purchased from Sigma-Aldrich. *N*,*N*-Dimethylformamide (DMF) was purchased from Fisher Scientific. All chemicals were used as received. $H_2$3PhT$_2$DC,[11] $H_2$3HT$_2$DC,[11] and H_2T_3DC[14] were prepared by literature procedures. THF was distilled from Na/benzophenone. ^{1}H NMR spectra were collected on either a Bruker AV-300 or AV-400 spectrometer and were referenced to residual solvent. EI mass spectra were obtained using a Kratos MS-50 mass spectrometer coupled to a MASPEC data system. Infrared spectra were obtained on a Thermo Nicolet 6700 with a Smart Orbit accessory in the range 4000−400 cm^{-1}. Thermogravimetric analyses (TGA) were performed using a Perkin-Elmer Pyris 6 thermogravimentric analyzer under a nitrogen atmosphere at a rate of 10 °C min^{-1}. Magnetization measurements

Received: May 24, 2013
Published: August 12, 2013

   dx.doi.org/10.1021/ic401305c | *Inorg. Chem.* 2013, 52, 10021−10030

Scheme 1

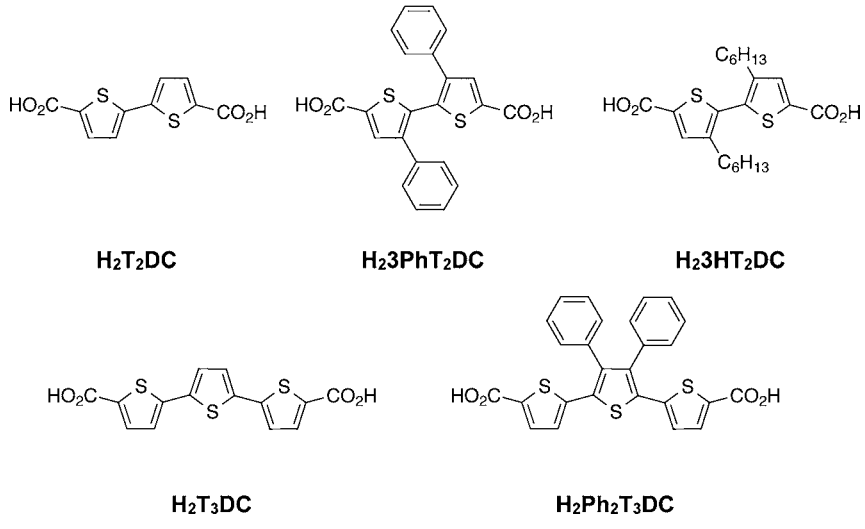

were performed using a Quantum Design MPMS-XL-7S SQUID magnetometer with an Evercool-equipped liquid helium dewar. Diamagnetic contributions to the magnetic susceptibility were corrected for using Pascal's constants.[19] CHN elemental analyses were performed using a EA1108 elemental analyzer. Powder X-ray diffraction (PXRD) patterns were obtained on a Bruker D8 Advance instrument at a scan rate of 5° min^{-1}. TOPOS[20] was used to determine net topology.

X-ray Crystallography. All crystals were mounted on glass fibers. Diffraction from **1** and **3** was measured on a Bruker APEX DUO diffractometer with graphite monochromated Cu Kα radiation. Diffraction from **2** and **4** was measured on a Bruker APEX DUO diffractometer with graphite monochromated Mo Kα radiation. Diffraction from **5** was measured on a Bruker X8 APEX II diffractometer with graphite monochromated Mo Kα radiation. Data were collected and integrated using the SAINT software package.[21] Data were corrected for absorption effects using the multiscan technique (SADABS).[22] Structures were solved using direct methods.[23] Non-hydrogen atoms were refined anisotropically except for atoms C37−C38, C43−C44, C59−C60, C84−C88, C107−C110, C130−C132, C137, C148−C150, N7, and O34 of **2**. All non-O−H hydrogens were placed in calculated positions; O−H hydrogens in **4** were found on the difference map while O−H hydrogens in **1**−**3** were not modeled. Refinements for **1**−**5** were performed using SHELXL-97[24] *via* the WinGX[25] interface. Compound **1** crystallizes with disordered coordinating and noncoordinating solvent at the O8 site, and the group was modeled in two orientations. Compound **2** crystallizes with significant disorder in one *n*-hexyl group (C17−C22), and the group was modeled in two orientations. Restraints on bond lengths for *n*-hexyl groups were employed to maintain reasonable geometries. There are regions of unresolved electron density in the void volume of compounds **1** and **2** that could not be appropriately modeled. The PLATON/SQUEEZE[26] program was used to generate a data set free of electron density in those regions. Crystallographic details for compounds **1**−**5** can be found in Table S3.

Synthesis. *3′,4′-Diphenyl-2,2′:5′,2″-terthiophene-5,5″-dicarboxylic Acid ($H_2Ph_2T_3DC$).* 3′,4′-Diphenyl-2,2′:5′,2″-terthiophene[27] (0.41 g, 1.0 mmol) was added to THF (20 mL). The flask was cooled to −78 °C, and *n*-butyllithium (1.3 mL, 2.1 mmol, 1.6 M in hexanes) was added dropwise. The yellow solution turned yellow-orange, and then green during the addition. The reaction mixture was warmed to and held at 0 °C for one hour, and then cooled to −78 °C. Addition of excess solid carbon dioxide pellets resulted in the formation of a vibrant orange opaque suspension. The reaction was allowed to warm to room temperature overnight. Water (20 mL) was added to quench the reaction. The aqueous layer was washed with diethyl ether (3 × 10 mL), and the product was precipitated by the addition of excess 1 M HCl, filtered, washed with 0.1 M HCl, methanol, diethyl ether, and finally dried *in vacuo* to afford an orange solid (87% yield). Mp > 300 °C. *m*/*z*: 488. ^{1}H NMR (300 MHz, d_6-DMSO) δ 7.56 (d, J = 3.9 Hz, 2 H), 7.29 (m, 6 H), 7.18 (m, 6 H). FT-IR (cm^{-1}) 3390 (w, br), 3052 (w) 2809 (w), 2521 (w, br), 1651 (s), 1513 (m), 1487 (w), 1440 (s), 1289 (m, br), 1112 (m), 1050 (w), 917 (w), 797 (m), 745 (m), 699 (s), 623 (w), 511 (m), 483 (w). Anal. Calcd for $C_{26}H_{16}O_4S_3$: C, 63.91; H, 3.30. Found: C, 63.46; H, 3.23.

*$[Mn(3PhT_2DC)(DMF)_{0.45}(H_2O)_{2.55}\cdot 1.55DMF]_n$ (**1**).* $MnCl_2\cdot 4H_2O$ (0.0198 g, 0.100 mmol) and $H_2$3PhT$_2$DC (0.0406 g, 0.100 mmol) were dissolved in DMF (5 mL). The solution was transferred to a 23 mL Teflon-lined Parr bomb and sealed. The vessel was heated to and held at 110 °C for 48 h, and then the bomb was cooled at a rate of 3.7 °C h^{-1}. Colorless crystals of $[Mn(3PhT_2DC)(DMF)_{0.45}(H_2O)_{2.55}\cdot 1.55DMF]_n$ were isolated in 73% yield. FT-IR (cm^{-1}): 3430 (w, br), 2933 (w, br), 1637 (s), 1570 (s), 1528 (m), 1494 (m), 1410 (s), 1372 (s), 1347 (s), 1209 (m), 1109 (m), 1062 (w), 869 (w), 846 (w), 765 (m), 698 (m), 628 (w), 550 (w), 497 (w). Anal. Calcd for $C_{28}H_{26}N_2O_{8.54}S_2Mn$: C, 52.09; H, 4.06; N, 4.34. Found: C, 52.03; H, 4.61; N, 4.71.

*$[Mn_6(3HT_2DC)_6(DMF)_3(H_2O)_5\cdot xDMF\cdot yH_2O]_n$ (**2**).* $MnCl_2\cdot 4H_2O$ (0.0198 g, 0.100 mmol) and $H_2$3HT$_2$DC (0.0422 g, 0.100 mmol) were dissolved in DMF (5 mL). The solution was transferred to a 23 mL Teflon-lined Parr bomb and sealed. The vessel was heated to and held at 110 °C for 48 h, and then the bomb was cooled at a rate of 3.7 °C h^{-1}. Colorless crystals of $[Mn_6(3HT_2DC)_6DMF)_3H_2O)_5\cdot xDMF\cdot yH_2O]_n$ were isolated in 56% yield. FT-IR (cm^{-1}): 2925 (m), 2854 (m), 1647 (m), 1565 (m), 1530 (m), 1421 (s), 1386 (s), 1353 (s), 1258 (w), 1195 (w), 1102 (m), 1016 (w), 871 (w), 774 (s), 714 (m), 677 (m), 484 (w). Anal. Calcd for $C_{141}H_{199}N_3O_{32}S_{12}Mn_6$: C, 53.55; H, 6.34; N, 1.33. Found: C, 54.40; H, 6.19; N, 2.44. (The discrepancy between the calculated and experimental elemental analysis is associated with the presence of noncoordinated solvent that was removed during the SQUEEZE protocol.)

*$[Mn(T_3DC)(H_2O)_2]_n$ (**3**).* $MnCl_2\cdot 4$ H_2O (0.0198 g, 0.100 mmol) and H_2T_3DC (0.0336 g, 0.100 mmol) were dissolved in DMF (5 mL). The solution was transferred to a 23 mL Teflon-lined Parr bomb and sealed. The vessel was heated to and held at 110 °C for 48 h, and then the bomb was cooled at a rate of 3.7 °C h^{-1}. Yellow-orange crystals of $[Mn(T_3DC)(H_2O)_2]_n$ were isolated in 81% yield. FT-IR (cm^{-1}): 3212 (m, br), 1547 (m), 1507 (s), 1439 (s), 1380 (s), 1111 (m), 1064 (w), 1034 (m). 858 (m), 785 (m), 769 (s), 699 (w), 676 (w), 631 (w), 534 (w), 476 (m). Anal. Calcd for $C_{14}H_9O_{5.5}S_3Mn$: C, 40.39; H, 2.18. Found: C, 39.63; H, 2.49.

*$[Mn(T_3DC)(H_2O)_{1.5}]_n$ (**4**).* Red-orange crystals of **4** were grown from the solvothermal reaction mixture of **3** and isolated in less than 1% yield. FT-IR (cm^{-1}): 3590 (w), 1641 (sh), 1626 (m), 1557 (s), 1530

dx.doi.org/10.1021/ic401305c | *Inorg. Chem.* 2013, 52, 10021−10030

(m), 1509 (m), 1446 (m), 1435 (m) 1361 (vs), 1128 (m), 1066 (m), 1031 (m), 866 (m), 767 (s), 680 (w), 642 (w), 541 (w), 483 (m).

*[Mn(Ph$_2$T$_3$DC)(DMF)$_2$]$_n$ (**5**).* $MnCl_2·4H_2O$ (0.0198 g, 0.100 mmol) and $H_2Ph_2T_3DC$ (0.0488 g, 0.100 mmol) were dissolved in DMF (5 mL). The solution was transferred to a 23 mL Teflon-lined Parr bomb and sealed. The vessel was heated to and held at 110 °C for 48 h, and then the bomb was cooled at a rate of 3.7 °C h^{-1}. Dark yellow crystals of $[Mn(Ph_2T_3DC)(DMF)_2]_n$ were isolated in 64% yield. FT-IR (cm^{-1}): 3089 (w), 2936 (w), 1639 (s), 1563 (s), 1528 (m), 1441 (m), 1379 (s), 1252 (m), 1213 (w), 1105 (m), 1069 (w), 1024 (w), 904 (w), 814 (m), 770 (s), 701 (m), 671 (m), 628 (w), 613 (w), 510 (w), 465 (m). Anal. Calcd for $C_{32}H_{28}N_2O_6S_3Mn$: C, 55.89; H, 4.10; N, 4.07. Found: C, 54.91; H, 4.09; N, 3.93.

RESULTS AND DISCUSSION

Synthesis. Oligothiophene dicarboxylic acid linkers (Scheme 1) were synthesized from Kumada cross coupling reactions followed by carboxylation of the α positions of the terminal thienyl groups. Compounds **1**−**3** and **5** were synthesized directly from solvothermal reactions of $MnCl_2·4H_2O$ and an oligothiophene dicarboxylic acid in DMF at 110 °C for 48 h. Solvothermal reaction times of 24 h or less gave minimal product, and fast cooling rates gave polycrystalline powder as the product. The low yield of **4** can be partially credited to most of the reactants being consumed in the formation of **3**. The slow emergence of **4** from the reaction mixture of **3** is ascribed to the formation of a kinetic product, whereas **3** may be the thermodynamic product of the reaction. Table 1 summarizes the preparation and dimensionality of **1**−**5**.

Table 1. Summary of Preparation and Structure Types

compd	preparation	dimensionality	inorganic building unit
1	solvothermal	2D	mononuclear
2	solvothermal	3D	linear trinuclear
3	solvothermal	3D	mononuclear
4	post-solvothermal	3D	mononuclear
5	solvothermal	1D	binuclear

Crystal Structures. *Bithiophene MOFs.* $[Mn(3PhT_2DC)(DMF)_{0.45}(H_2O)_{2.55}·1.55DMF]_n$ (**1**) forms 2D sheets along the crystallographic *ac*-plane. Each asymmetric unit (Figure 1a) contains $^1/_2$ Mn1, $^1/_2$ Mn2, one 3PhT$_2$DC^{2-} linker, two coordinating H_2O, one noncoordinating DMF, and a disordered site that is either coordinating water and noncoordinating DMF (55% occupancy) or coordinating DMF (45% occupancy). Both manganese sites adopt an octahedral geometry: Mn1 is coordinated to two *trans* monodentate carboxylates (O1) and four solvent molecules (H_2O and DMF), while Mn2 is coordinated to four μ_2-η^1:η^1 carboxylates (O3 and O4) and two solvent molecules. Figure S1a shows the linker coordination of 3PhT$_2$DC^{2-} within **1**. *Syn*−*anti* carboxylates bridge Mn2 centers to form Mn−carboxylate chains along the *c*-axis, and each Mn2 is 4.52(1) Å from the nearest Mn2. Mn1 sites are not linked directly *via* carboxylate bridges, and the distance between two Mn1 atoms is 9.04(2) Å. Mn1 effectively acts as a bridge for the Mn2 nodes *via* 3PhT$_2$DC^{2-} linkers. The extended structure of **1** and the linkage of the manganese environments are shown in Figure 1b. The 3PhT$_2$DC^{2-} linker is twisted with a torsion angle of 122.49(2)°: the phenyl groups are flanked away from each other and do not engage in intermolecular interactions. Noncoordinating solvent and phenyl rings occupy the void space in the solid state structure.

The structure of **1** can be reduced to a 4-connected uninodal net with **sql**-Shubnikov tetragonal plane net topology. Previously synthesized MOFs containing this linker[11] are also 2D frameworks; changing the metal center thus far has not caused changes in dimensionality of 3PhT$_2$DC^{2-} MOFs. Literature precedent[27,28] for the solid state structure of 3,3′-diphenyl-2,2′-bithiophene and its derivatives[11] suggests that the conformations that are accessible in the solid state will lead to 3PhT$_2$DC^{2-} having a linking angle of 140−150°. Ligands with such linking angles alone are not conducive to forming 3D frameworks.[29] The presence of additional driving forces (e.g., van der Waals interactions, π−π stacking) may help overcome the disfavored linking angle to form structures with higher dimensionality.

A 3D framework belonging to the acentric orthorhombic space group $C222_1$ is formed upon crystallization of $[Mn_6(3HT_2DC)_6(DMF)_3(H_2O)_5·x\text{DMF}·yH_2O]_n$ (**2**). The metal nodes of **2** consist of linear trinuclear manganese centers coordinated to 3HT$_2$DC^{2-} linkers, DMF, and H_2O. Terminal−center manganese distances range from 3.702(3) to 3.748(3) Å. The four terminal manganese atoms in the asymmetric unit are coordinated to two solvent molecules each (Mn1, Mn4, and Mn6 are coordinated to a DMF and H_2O, while Mn3 is coordinated to two H_2O molecules), a μ_2-η^2:η^1 carboxylate, and two μ_2-η^1:η^1 carboxylates. The central manganese atom is coordinated to six oxygens from six unique 3HT$_2$DC^{2-} linkers. Four of the oxygens belong to carboxylates that coordinate in a μ_2-η^1:η^1 mode. The other two oxygens belong to carboxylates that bind in a μ_2-η^2:η^1 fashion and coordinate to the terminal manganese in addition to the central manganese atom. Mn−O bond lengths are typical: Mn−O carboxylate bond lengths range from 2.14 to 2.22 Å, while Mn−O solvate bond lengths range from 2.06 to 2.27 Å. The six 3HT$_2$DC^{2-} within **2** have annular torsion angles in the regimes of 55° and 90°. Previous theoretical studies calculate the torsion angle of 3,3′-dihexyl-2,2′-bithiophene to be 72°,[30] suggesting the *n*-hexyl chains will drive the thiophene rings of 3HT$_2$DC^{2-} to near perpendicular angles. 3HT$_2$DC^{2-} adopts two coordination modes within the solid state structure of **2**. Two linkers in the asymmetric unit have carboxylates that coordinate in a bis-bidentate fashion (Figure S1b) while the other four 3HT$_2$DC^{2-} linkers in the asymmetric unit coordinate with a bidentate μ_2-η^1:η^1 mode and a chelating-bridging μ_2-η^2:η^1 mode (Figure S1c). The six coordinating 3HT$_2$DC^{2-} linkers bind to four other trinuclear metal nodes. As illustrated in Figure 2, two 3HT$_2$DC^{2-} connect to two separate nodes, whereas two sets of two 3HT$_2$DC^{2-} act as a twisted double pillar and link to one node each.

Compound **2** has a 4-connected uninodal **lvt** net topology and a Schläfli symbol of $4^2.8^4$ when the trinuclear cluster is treated as a single node. *n*-Hexyl chains, some of which are disordered, and noncoordinating solvent fill the voids of the coordination polymer. There is at least one noncoordinating DMF in the asymmetric unit, but the exact number and composition of solvent molecules could not be determined. The *n*-hexyl chains of the linkers are not evenly distributed within the free space of **2** and appear to cluster within this structure. Exact determination of the extent of aggregation cannot be assessed due to the disorder of the *n*-hexyl chains. However, intraligand repulsion and interligand aliphatic attraction contribute to the twisting of the 3HT$_2$DC^{2-} linker and observed grouping of *n*-hexyl chains.

The long-range configuration of **2** (Figure 2) is dissimilar to other bithienyl manganese coordination polymers. Compound

dx.doi.org/10.1021/ic401305c | Inorg. Chem. 2013, 52, 10021−10030

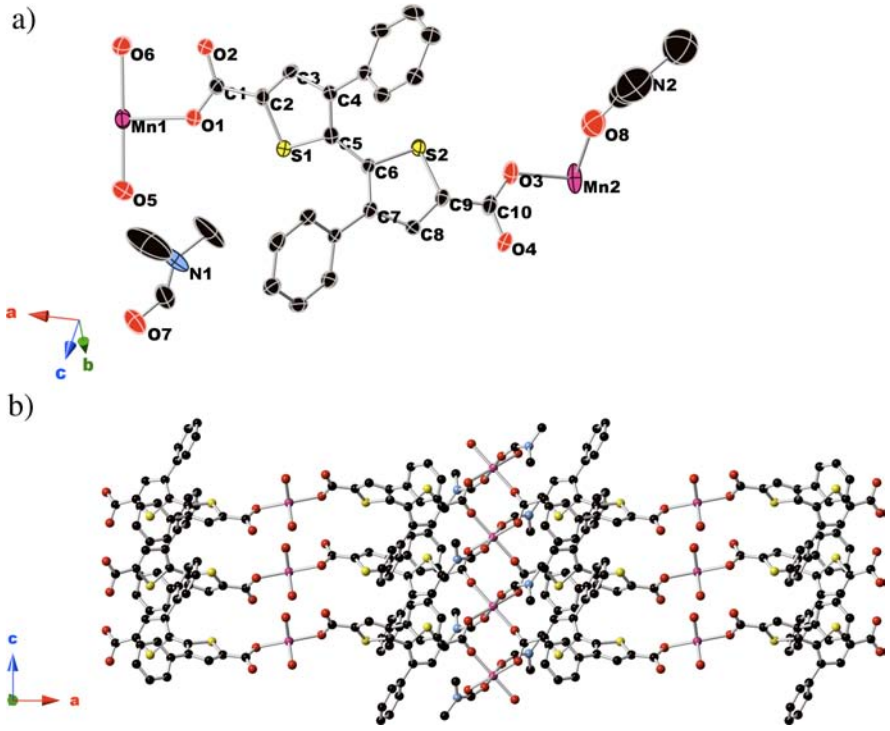

Figure 1. Solid state structure of **1**. (a) Asymmetric unit of **1**. (b) Extended view of **1** on the *ac*-plane.

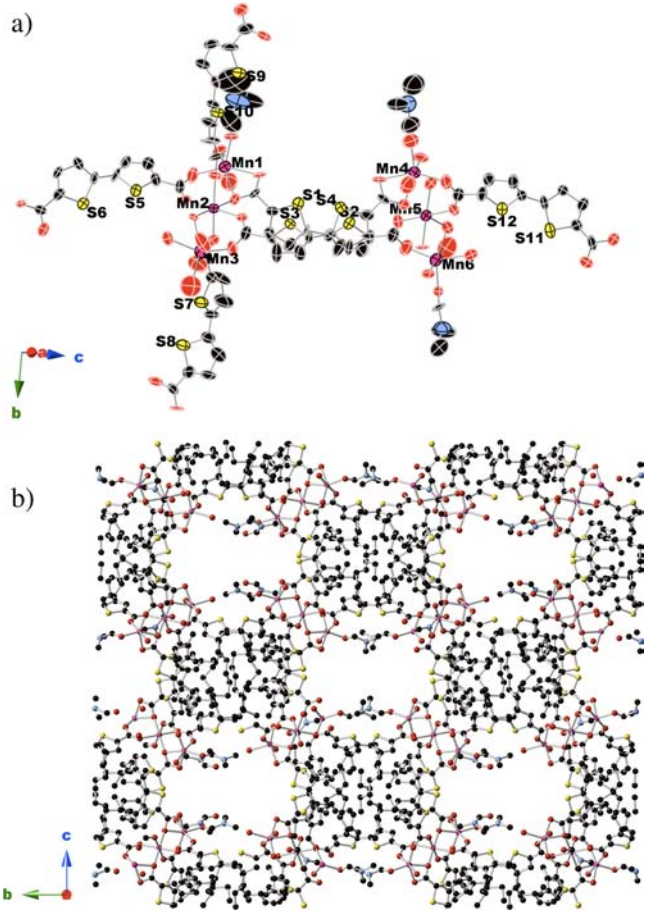

Figure 2. Solid state structure of **2**. (a) Asymmetric unit with *n*-hexyl chains removed for clarity. (b) Extended structure of **2** viewed from the *bc*-plane.

1 has phenyl substituents at the β position and is a 2D sheet, whereas a Mn^{2+} MOF with unsubstituted bithiophenes, $[Mn_3(T_2DC)_3(DMF)_4]_n$[13] (2,2′-bithiophene-5,5′-dicarboxylic acid), has **sxb** topology and trinuclear centers that are similar to those in **2**. Although the two compounds share inorganic building units, each trinuclear center of $[Mn_3(T_2DC)_3(DMF)_4]_n$ is linked to six other centers, whereas **2** is linked to four other centers. Figure 3a illustrates the simplified coordination of the trinuclear nodes for **2** and $[Mn_3(T_2DC)_3(DMF)_4]_n$. This change in the linkage of the metal centers has a drastic effect on the overall topology. As illustrated in Figure 3b, the 4-connected **lvt** net topology of **2** is vastly different from the 6-connected **sxb** topology of $[Mn_3(T_2DC)_3(DMF)_4]_n$. The change in topology is attributed to van der Waals attraction of the *n*-hexyl chains[11,18] to other *n*-hexyl chains that directs the extended structure of **2**. This interaction between chains causes the linkers to twist in a way that changes the linking angle of the carboxylates which influences the position and orientation of metal centers.

Terthiophene MOFs. The T_3DC^{2-} linker has been previously used to form a copper−T_3DC metal−organic polyhedron with the T_3DC^{2-} linker in a *cis,cis* conformation and at a 90° linking angle.[14] However, there have been no reports of crystallographically characterized structures with terthiophene linkers in a metal−organic *framework* or coordination polymer.

Reaction of $MnCl_2{\cdot}4H_2O$ and H_2T_3DC under solvothermal conditions affords two distinct products: compounds **3** ($[Mn(T_3DC)(H_2O)_2]_n$) and **4** ($[Mn(T_3DC)(H_2O)_{1.5}]_n$). Both are 3D frameworks of Mn^{2+}, T_3DC^{2-}, and coordinating H_2O. The bulk material, **3**, crystallizes in the acentric orthorhombic space group $P2_12_12_1$. The asymmetric unit shown in Figure 3 contains one Mn^{2+}, one T_3DC^{2-}, and two coordinating terminal water molecules. The carboxylate and water oxygens form an octahedral coordination environment

dx.doi.org/10.1021/ic401305c | *Inorg. Chem.* 2013, 52, 10021−10030

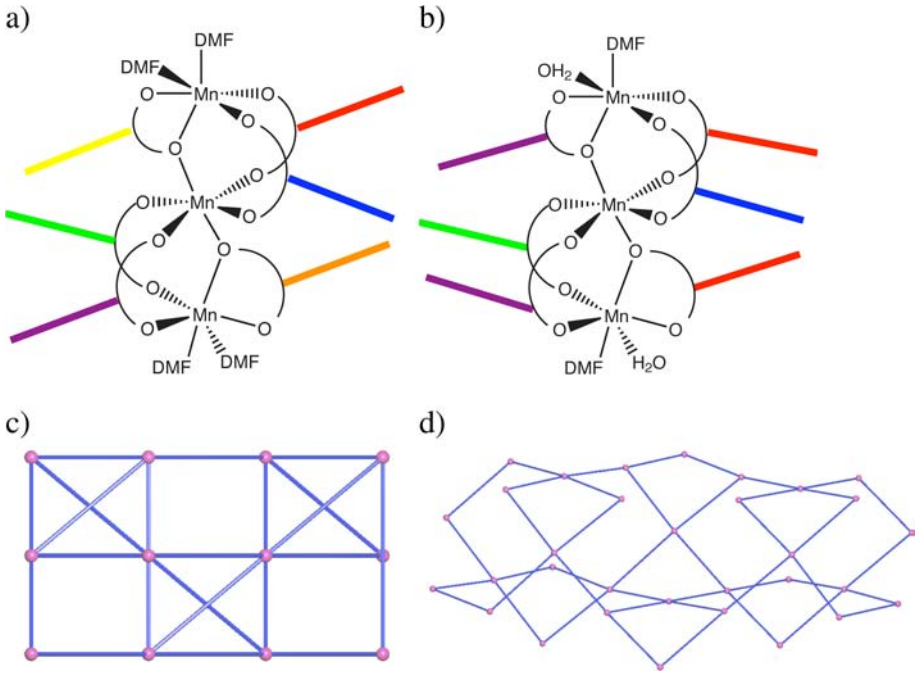

Figure 3. Simplified coordination environments for the manganese trinuclear nodes of (a) 6-connected $[Mn_3(T_2DC)_3(DMF)_4]_n$ and (b) 4-connected compound **2**. Colored rods illustrate bithienyl linkers with rods of the same color going to the same trinuclear node. Net topology of (c) $[Mn_3(T_2DC)_3(DMF)_4]_n$ and (d) **2**.

around the manganese. The T_3DC^{2-} linker adopts a μ_2-η^1:η^1 (Figure S1b) binding mode. The *syn*−*anti* carboxylate-bridged Mn−Mn distances are 4.73(2) and 5.04(2) Å. Mn−O carboxylate distances are 2.142(9)−2.192(8) Å, and Mn−O water distances are 2.177(9) and 2.207(9) Å. The *trans,cis* thiophene rings of **3** have only moderate coplanarity: the S1−C5−C6−S2 torsion angle is 157.9(9)°, and the S2−C9−C10−S3 torsion angle is 19.8(9)°. The extended structure in Figure 4b,c shows that the manganese centers form a 2D lattice that are connected by T_3DC^{2-} linkers along the *c*-axis. When the manganese centers are treated as nodes, the simplified framework has a 4-connected **lvt** topology similar to that of **2**.

Crystals of **4** were grown from the reaction mother liquor of **3**. Compound **4** crystallizes in the monoclinic space group *C*2/*c* and is a 3D framework (Figure 5). The asymmetric unit consists of one T_3DC^{2-} linker, one Mn, one coordinating terminal water molecule, and half of a bridging water molecule. Figure 5a shows the asymmetric unit of **4**. Two bis-monodentate carboxylate oxygens (O1 and O2), a μ_2:η^2 carboxylate (O3 and O4), one terminal water, and one bridging water coordinate to the manganese center in an octahedral geometry. Figure S1a shows the T_3DC^{2-} coordination mode, and Figure 5c shows the simplified coordination environment for the manganese center. The μ_2-η^2 Mn−O bond lengths are slightly elongated (2.199(5)−2.225(5) Å) compared to the bis-monodentate Mn−O bond (2.120(5)−2.144(5) Å). Similarly, the terminal H_2O Mn−O bond is 2.157(5) Å compared to 2.262(4) Å for the bridging H_2O Mn−O bond. The manganese centers are rather close to each other with separation distances of 3.379(7) and 3.731(7) Å.

The rings of the terthiophene linker of **4** are nearly coplanar. The S1−C5−C6−S2 torsion angle is 179.2(4)°, and the S2−C9−C10−S3 torsion angle is −178.8(4)° giving a *trans,trans* conformation to the linker. The extended structure of **4** shows that the T_3DC^{2-} linkers are stacked in parallel pairs and are separated by 3.526(8) Å (S2−S2 contact) to 3.572(9) Å (terminal ring centroid−centroid) (Figure 5b). These coplanar pairs arrange in a herringbone orientation throughout the coordination polymer. When the manganese center and

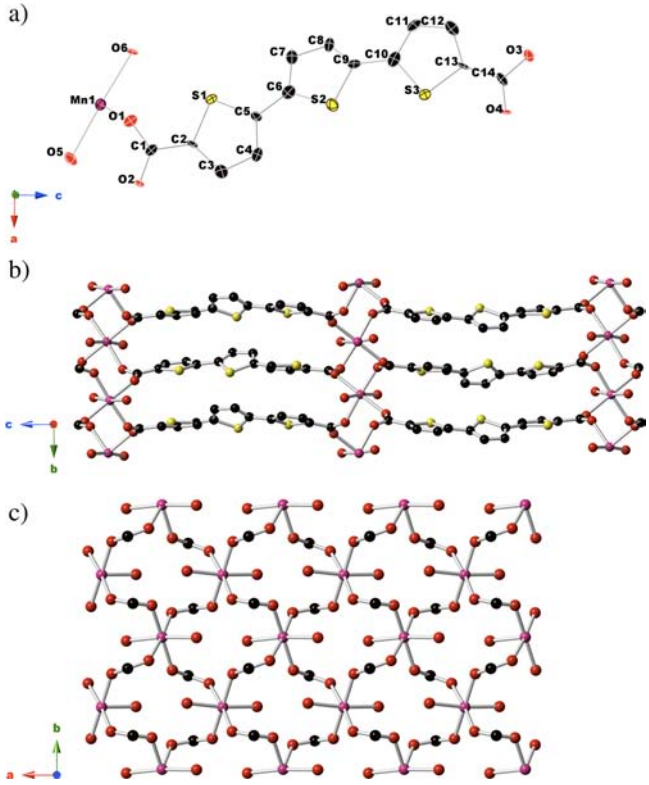

Figure 4. Structure of **3**. (a) The asymmetric unit of **3**. (b) View of the extended structure along the *a*-axis. (c) View of the carboxylate-bridged 2D lattice of Mn^{2+} centers with terthiophene units removed for clarity.

dx.doi.org/10.1021/ic401305c | *Inorg. Chem.* 2013, 52, 10021−10030

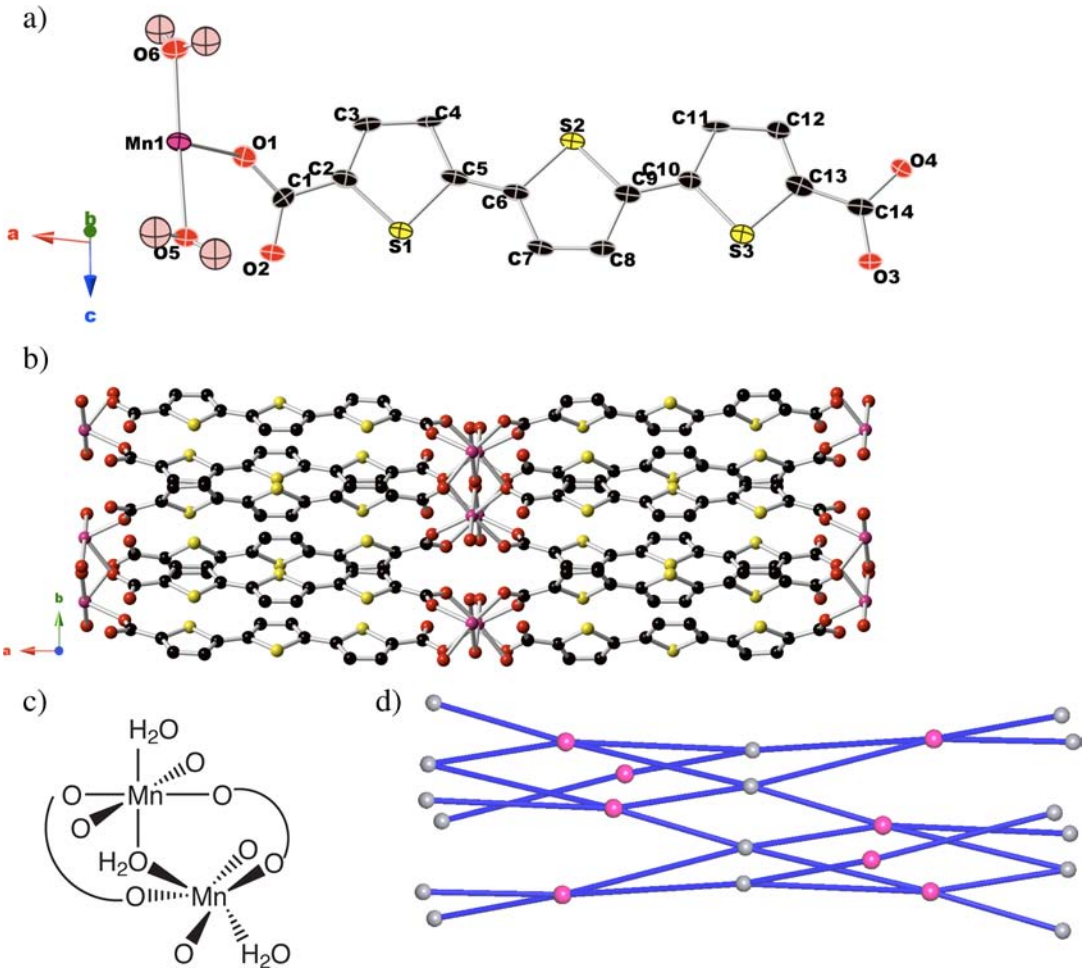

Figure 5. (a) Asymmetric unit of **4**. (b) The extended framework of **4**. (c) The simplified coordination environment of the manganese center in **4**. (d) Simplified topology of **4**. Gray nodes, Mn; pink nodes, terthiophene.

T_3DC^{2-} are treated as nodes, the simplified framework has a 4-connected **umc** topology (Figure 5d) and is assigned the Schläfli symbol of $4^3.6^2.8$.

The stacking and orientations of **3**, **4**, and 2,2′:5′,2′′-terthiophene (T_3)[31] differ from each other in the solid state. The thiophene rings of T_3 deviate 6−9° from planarity, and the closest S−S contact is 3.70 Å. T_3 molecules crystallize in a herringbone orientation and do not engage in any close $\pi-\pi$ interaction. These new terthiophene dicarboxylate MOFs, along with the copper−T_3DC metal−organic polyhedron, demonstrate the structural versatility of the T_3DC^{2-} linker. In particular, linkers in coordination polymer **4** are more planar and have closer S−S contacts than in the parent molecule T_3.

β substitution of phenyl groups on the central thiophene ring of the terthiophene linker was explored, resulting in the synthesis of $H_2Ph_2T_3DC$ and subsequently $[Mn(Ph_2T_3DC)(DMF)_2]_n$ (**5**). This coordination network crystallizes in the triclinic space group $P\bar{1}$ and is composed of 1D chains. Figure 6 shows the metal center coordination as well as the extended structure of **5**. The binding modes of **5** are depicted in Figure S1e. The chains consist of alternating binuclear manganese clusters and two $Ph_2T_3DC^{2-}$ linkers. Two bis-monodentate carboxylate oxygens, two bidentate carboxylate oxygens, and two DMF molecules adopt a distorted octahedral geometry around each crystallographically equivalent manganese center. The Mn−O distances are 2.1296(9)−2.1367(9) Å for the monodentate carboxylate oxygens, 2.150(1)−2.163(1) Å for the DMF oxygens, and 2.2339(9)−2.3322(9) Å for the bidentate carboxylate oxygens. The manganese atoms in the binuclear cluster are separated by 4.505(2) Å.

The *cis,trans* thiophene rings of **5** are less coplanar than **3** and **4**: the S1−C5−C6−S2 torsion angle is 38.49(6)°, and the S2−C9−C10−S3 torsion angle is 150.35(7)°. On the basis of the C1-central thiophene centroid-C14 angle, the linking angle of $Ph_2T_3DC^{2-}$ deviates 40° from linearity. The twisted conformation of the linker in the solid state and consequential dimensionality can be connected to the presence of the bulky phenyl groups at the β position of the central thiophene ring.

Overall, compounds **1**−**5** demonstrate a sampling of the crystallographic environments available to oligothiophenes within a coordination polymer. Although the oligothiophene ligands have similar linking angles, the presence of phenyl and *n*-hexyl functional groups controls the dimensionality of the extended structures. In addition, compounds containing terthiophene derivatives are not mere extensions of the bithiophene analogues. One striking difference between the bithiophene compound $[Mn_3(T_2DC)_3(DMF)_4]_n$ and terthiophene compounds **3** and **4** is that the terthiophene compounds form rather dense frameworks lacking noncoordinating solvent. The propensity for linear trinuclear clusters to form for MOFs containing bithiophene linkers ($[Mn_3(T_2DC)_3(DMF)_4]_n$ and

dx.doi.org/10.1021/ic401305c | *Inorg. Chem.* 2013, 52, 10021−10030

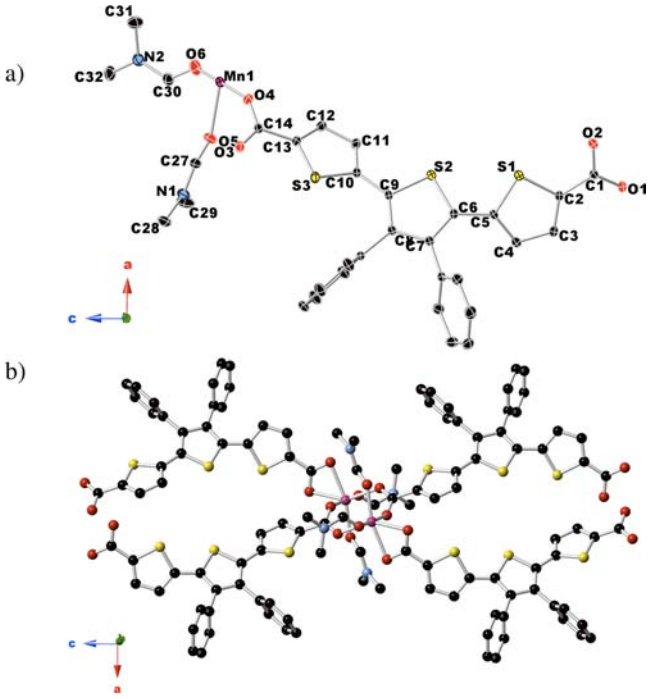

Figure 6. Solid state structure of **5**. (a) Asymmetric unit. (b) Binuclear metal center.

2) versus mononuclear extended frameworks for terthiophene-containing compounds (**3** and **4**) is still under investigation.

Powder X-ray Diffraction, Thermogravimetric Properties, and Infrared Spectroscopy. The phase purity of compounds **1**−**5** was determined using powder X-ray diffraction (PXRD). The diffraction patterns were compared to the predicted diffraction patterns from the structure determined by single crystal X-ray crystallography (Figure S2). For compounds **1** and **3**−**5**, the predicted and experimental powder patterns of the bulk material match well. Due to the small quantity of **4** that was available for analysis, some peaks in the diffraction pattern of **4** are weaker than expected but still present. The peaks of the experimental diffraction pattern of **2** are broad compared to the predicted pattern, and a loss of crystallinity is credited to structural collapse upon desolvation of the bulk material.

Thermogravimetric analysis (TGA) was performed on **1**−**3** and **5** to determine the thermal stability and evaluate the composition of these materials (Figure S3). A summary of the analyses is given in Table S1. Noncoordinated solvent is lost between 50 and 120 °C followed by the loss of coordinating solvent near 200 °C. Combustion of organic material occurs before 400 °C for one- and two-dimensional coordination polymers **1** and **5** and by 450 °C for three-dimensional frameworks **2** and **3**. PXRD was used to determine the identity of the decomposition products; a mixture of Mn_3O_4, MnOS, and trace amounts of other compounds that could not be identified were found.

Infrared spectroscopy was used to confirm the carboxylate binding modes observed in **1**−**5**.[32] The results are summarized in Table S2. In **1**, the weak C═O stretches anticipated for a noncoordinated oxygen belonging to a η^1 carboxylate are overwhelmed by the C═O stretch of DMF. The noncoordinated oxygen belonging to the μ_2:η^2 carboxylate of **4** has distinct IR stretches at 1626 and 1641 cm^{-1}. These stretches are absent in **3**.

Magnetic Properties. Bulk magnetic susceptibilities of polycrystalline samples of compounds **1**−**3** and **5** were measured at 10 kOe in the temperature range 2−300 K.

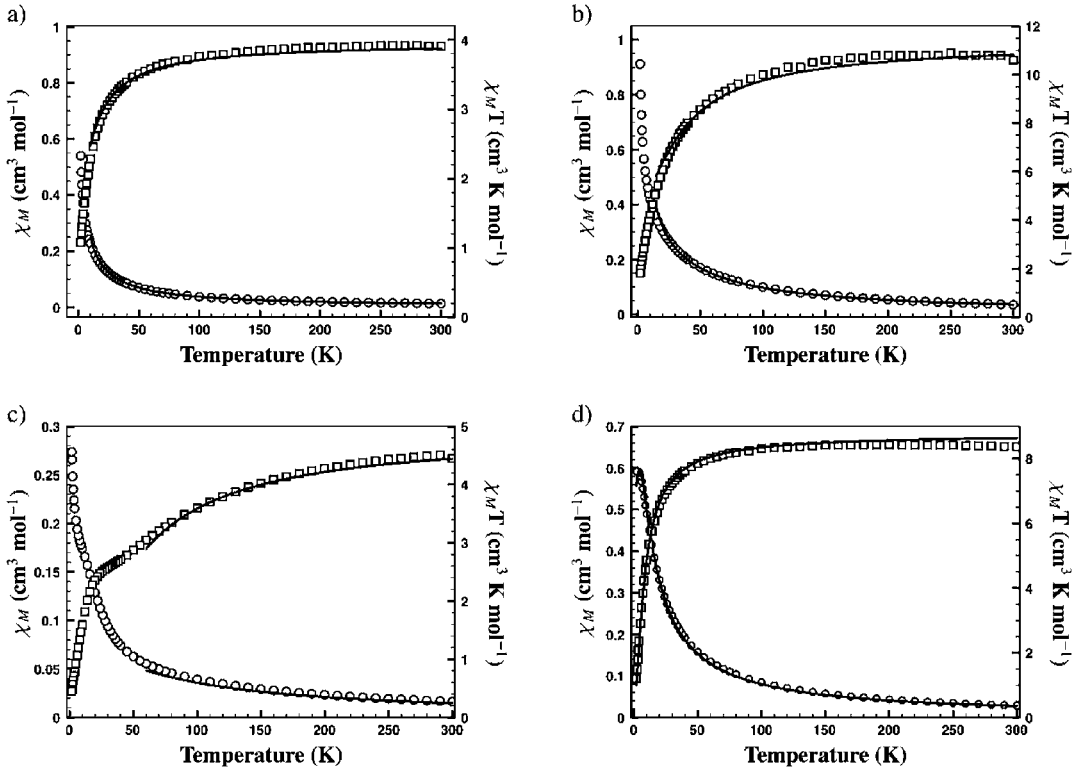

Figure 7. χ_M vs T (○); $\chi_M T$ vs T (□) for **1**−**3** and **5**. The solid lines show the best theoretical fit.

dx.doi.org/10.1021/ic401305c | Inorg. Chem. 2013, 52, 10021−10030

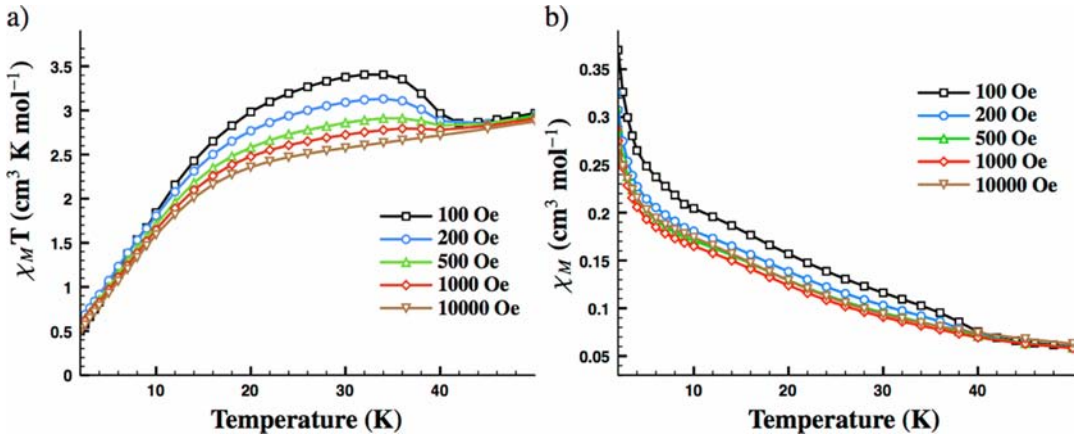

Figure 8. Low temperature magnetic susceptibility data for **3**: (a) $\chi_M T$ vs T and (b) χ_M vs T at various fields.

Compound **4** could not be synthesized in sufficient quantities to perform magnetic susceptibility measurements. The results of these experiments are shown in Figure 7.

Compound **1** consists of both isolated Mn^{2+} centers (Mn1) and carboxylate-bridged 1D Mn^{2+} chains (Mn2). Antiferromagnetic behavior, shown in Figure 7a, was observed down to 2 K. At 300 K, the magnetic susceptibility is 3.91 cm^3 K mol^{-1} which is less than the expected value of 4.37 cm^3 K mol^{-1} for one isolated Mn^{2+} center. A Curie constant of C = 4.18 cm^3 mol^{-1} and a Weiss constant of θ = −8.57 K were found, suggesting the material is antiferromagnetic.

The distance between the carboxylate-bridged Mn2−Mn2 centers of **1** is 4.52(1) Å, while the Mn1−Mn1 centers are well separated by 9.04(2) Å. It can be assumed that there is insignificant interchain interaction or exchange between the Mn1 centers. The molar magnetic susceptibility of **1** can be modeled as:

$$\chi_M = \frac{1}{2}(\chi_{chain} + \chi_{paramagnet}) \quad (1)$$

where χ_{chain} describes the Mn2−Mn2 interaction *via* the Fisher infinite chain model[33] (eq 2):

$$\chi_{chain} = \frac{N_A g^2 \mu_B^2 S(S+1)}{3k_B T}\left[\frac{1+U}{1-U}\right] \quad (2)$$

where U is the Langevin function:

$$U = \coth\frac{JS(S+1)}{k_B T} - \frac{k_B T}{S(S+1)} \quad (3)$$

and $\chi_{paramagnet}$ (eq 4) accounts for the contribution of the mononuclear Mn1 center:

$$\chi_{paramagnet} = \frac{N_A g^2 \mu_B^2 S(S+1)}{3k_B T} \quad (4)$$

Applying this model to the experimental magnetic susceptibility data between 300 and 10 K gives g = 1.983(2) and J = −2.00(3) cm^{-1} which confirms the antiferromagnetic behavior of **1**.

At 300 K, the experimental $\chi_M T$ value for **2** is 10.64 cm^3 mol^{-1} K which is below the value expected for three isolated Mn^{2+} centers. (The molecular weight used to calculate magnetic susceptibilities does not account for the non-coordinated solvent that could not be resolved crystallographically.) Compound **2** adheres to the Curie−Weiss law down to 15 K, at which point χ_M^{-1} deviates from linearity. The antiferromagnetic behavior of **2** is demonstrated by a Curie constant of C = 11.60 cm^3 mol^{-1} and a Weiss constant of θ = −17.00 K.

The large distances between trinuclear clusters (12.86(3) Å) and the terminal manganese within a trinuclear cluster (7.43(2) Å) are presumed to negate any significant magnetic coupling: their interactions are assumed to be zero. Although the terminal manganese atoms are in crystallographically unique locations, the similar chemical environments and distances to the central manganese atoms are sufficient grounds for treating the terminal manganese as equivalent species. Given these assumptions, the Hamiltonian for these trinuclear clusters is given in eq 5:

$$\hat{H} = -2J(\hat{S}_1\cdot\hat{S}_2 + \hat{S}_2\cdot\hat{S}_3) \quad (5)$$

The appropriate energy terms[34] are inserted into the van Vleck equation[35] (eq 6):

$$\chi_M = \frac{N_A g^2 \mu_B^2}{3k_B T}\cdot\frac{\Sigma S(S+1)(2S+1)\exp(-E/k_B T)}{\Sigma(2S+1)\exp(-E/k_B T)} \quad (6)$$

where:

$$E = \frac{JS(S+1)}{2}$$

per mole of metal ions. Modeling of the magnetic susceptibility data between 300 and 15 K gives values of g = 2.094(3) and J = −2.88(3) cm^{-1} (Figure 7b). These values are similar to those for other trinuclear manganese systems.[36] Although **2** belongs to an acentric space group, the magnetic behavior of the material does not reflect this crystallographic assignment. The lack of anisotropy or spin canting at low temperature can be associated with the loss of acentricity upon removal from a solvent-rich environment. Structural collapse and a loss of crystallinity are observed in the bulk polycrystalline sample (Figure S2b).

Compound **3** also crystallizes in an acentric space group and shows a significant deviation from normal antiferromagnetic behavior below 60 K. At 300 K, the experimental $\chi_M T$ value is 4.45 cm^3 mol^{-1} K, which is slightly higher than expected for an isolated Mn^{2+} center. A Curie constant of C = 5.18 cm^3 mol^{-1} and Weiss constant of θ = −43.03 K were found between 60 and 300 K indicating strong antiferromagnetic interactions within this temperature range (Figure 7c). Above 60 K, the

dx.doi.org/10.1021/ic401305c | *Inorg. Chem.* 2013, 52, 10021−10030

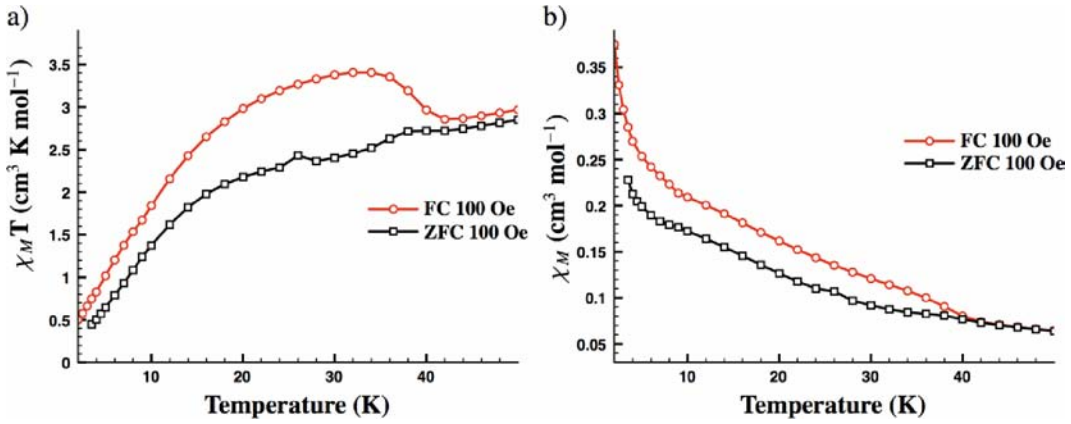

Figure 9. FC and ZFC magnetization plots for **3**: (a) $\chi_M T$ vs T and (b) χ_M vs T at 100 Oe.

magnetic coupling within the 2D lattice can be modeled using eq 7

$$\chi_M = \frac{N_A g^2 \mu_B^2 S(S+1)(1+U)^2}{3k_B T(1-U)^2} \quad (7)$$

where U is the previously defined Langevin function (eq 3). Least-squares analysis of the magnetic susceptibility data gives $g = 2.135(6)$ and $J = -1.94(3)$ cm^{-1} which confirms that the 2D sheets of metal centers are coupled antiferromagnetically.

To help describe the change in magnetic behavior below 60 K, variable field magnetic susceptibilities were measured (Figure 8). At lower fields, χ_MT increases slightly to a maximum found at 32 K before decreasing quickly again. This behavior is mostly saturated at 10 kOe. Below 25 K, saturation effects or antiferromagnetic interactions take over, and a minimum value of 0.50 cm^3 K mol^{-1} is reached at 2 K. This behavior is attributed to spin canting[37] which is a common phenomenon for materials without an inversion center.[38] Figure S4 shows that no remnant magnetization is observed at 2 K, and the M vs H curve does not increase rapidly at low field, suggesting that no ferromagnetic ordering is present at 2 K. To further elucidate the identity of the magnetic transition, zero-field cooled (ZFC) and field cooled (FC) magnetic susceptibility data were collected at 100 Oe (Figure 9). While the $\chi_M T$ versus T FC data show a prominent feature in $\chi_M T$ 20–40 K followed by a rapid decrease upon further cooling, the ZFC cooled data show monotonically decreasing values of $\chi_M T$ between 20 and 40 K before decreasing rapidly. Divergence of the ZFC and FC data below $T_c = 40$ K demonstrates the irreversibility of the magnetic transition originating from a magnetically ordered canted state. Convergence of behavior below 20 K suggests that antiferromagnetic interactions dominate in this regime.

The plots of χM and $\chi_M T$ versus T for compound **5** are shown in Figure 7d. Upon cooling from 300 K, $\chi_M T$ is 8.37 cm^3 mol^{-1} K at 300 K, which is less than the expected value for two isolated Mn^{2+} centers. The temperature dependence of χ_M^{-1} obeys the Curie–Weiss law above 10 K with a Curie constant of $C = 8.61$ cm^3 mol^{-1} and a Weiss constant of $\theta = -5.14$ K. The Hamiltonian for a homospin binuclear system[35] is given in eq 8:

$$\hat{H} = -J\hat{S}_1 \cdot \hat{S}_2 \quad (8)$$

For a binuclear system, the van Vleck equation (eq 9) takes the form of:

$$\chi_M = \frac{2N_A g^2 \mu_B^2}{k_B T} \cdot \frac{\Sigma S(S+1)(2S+1)\exp(-E/k_B T)}{\Sigma(2S+1)\exp(-E/k_B T)} \quad (9)$$

Following the Hamiltonian for a homospin binuclear system, least-squares analysis of the magnetic susceptibility data gave $g = 2.004(2)$ and $J = -0.594(5)$ cm^{-1}, showing that the Mn^{2+} are weakly coupled through the carboxylate bridges of the binuclear cluster.

CONCLUSIONS

A series of new bithiophene and terthiophene manganese metal–organic frameworks have been synthesized and characterized. Compounds **3**–**5** are the first examples of crystallographically characterized terthiophene coordination polymers. Compound **3** is found to be the major product of the reaction of $MnCl_2 \cdot 4H_2O$ and H_2T_3DC under solvothermal conditions, while **4** crystallizes from the reaction mother liquor. This work has shown that alkyl chains cluster in the otherwise void space of the MOFs. These interactions cause the thiophene rings to twist to near perpendicular angles and help to shape the topology of the extended structure. Similarly, phenyl groups do not provide any driving force for forming a particular extended structure and cause the linker to have the wrong geometry for forming 3D frameworks. The magnetic behavior of the manganese MOFs are sensitive to both the short-range and extended structure. Compounds **1**–**3** and **5** exhibit antiferromagnetic behavior and are well modeled by the given equations that describe the coordination environments. Current investigations are underway to elucidate the solid state structures and photophysical properties of d^{10} Zn^{2+} terthiophene MOFs.

ASSOCIATED CONTENT

Supporting Information

Crystallographic data, linker coordination modes, TGA traces for **1**–**3** and **5**, field dependence on the magnetization of **3**, selected tabulated IR data, and crystallographic data in CIF format. This material is available free of charge via the Internet at http://pubs.acs.org.

AUTHOR INFORMATION

Corresponding Author

*E-mail: mwolf@chem.ubc.ca. Phone: (604) 822-1702. Fax: (604) 822-2847.

Notes

The authors declare no competing financial interest.

■ ACKNOWLEDGMENTS

We thank the Natural Sciences and Engineering Research Council (NSERC) of Canada for funding this research. L.D.E. thanks D. Savard (Simon Fraser University) for assistance with collecting the magnetic susceptibility data.

■ REFERENCES

(1) *Handbook of Thiophene-Based Materials: Applications in Organic Electronics and Photonics*; Perepichka, I. F., Perepichka, D. F., Eds.; Wiley: West Sussex, 2009.

(2) Fichou, D. *J. Mater. Chem.* **2000**, *10*, 571−588.

(3) (a) Yassar, A.; Moustrou, C.; Youssoufi, H. K.; Samat, A.; Guglielmetti, R.; Garnier, F. *Macromolecules* **1995**, *28*, 4548−4553. (b) Wagner, P.; Ballantyne, A. M.; Jolley, K. W.; Officer, D. L. *Tetrahedron* **2006**, *62*, 2190−2199.

(4) Jeong, S.; Song, X.; Jeong, S.; Oh, M.; Liu, X.; Kim, D.; Moon, D.; Lah, M. S. *Inorg. Chem.* **2011**, *50*, 12133−12140.

(5) (a) Martínez Casado, F. J.; Fabelo, O.; Rodríguez-Velamazán, J. A.; Ramos Riesco, M.; Rodríguez Cheda, J. A.; Labrador, A.; Rodríguez-Blanco, C.; Campo, J.; Sánchez-Alarcos, V.; Müller, H. *Cryst. Growth Des.* **2011**, *11*, 4080−4089. (b) García-Couceiro, U.; Castillo, O.; Cepeda, J.; Lanchas, M.; Luque, A.; Pérez-Yáñez, S.; Román, P.; Vallejo-Sánchez, D. *Inorg. Chem.* **2010**, *49*, 11346−11361. (c) Manna, S. C.; Zangrando, E.; Drew, M. G. B.; Ribas, J.; Chaudhuri, N. R. *Eur. J. Inorg. Chem.* **2006**, 481−490. (d) Ma, L.-F.; Wang, L.-Y.; Wang, Y.-Y.; Du, M.; Wang, J.-G. *CrystEngComm* **2009**, *11*, 109−117. (e) Wang, X.-W.; Dong, Y.-R.; Zheng, Y.-Q.; Chen, J.-Z. *Cryst. Growth Des.* **2007**, *7*, 613−615.

(6) (a) Kar, P.; Haldar, R.; Gómez-García, C. J.; Ghosh, A. *Inorg. Chem.* **2012**, *51*, 4265−4273. (b) Liu, D.; Zhou, Q.; Chen, Y.; Yang, F.; Yu, Y.; Shi, Z.; Feng, S. *Cryst. Growth Des.* **2010**, *10*, 2661−2667.

(7) Zhu, Q.-Y.; Wang, J.-P.; Qin, Y.-R.; Shi, Z.; Han, Q.-H.; Bian, G.-Q.; Dai, J. *Dalton Trans.* **2011**, *40*, 1977−1983.

(8) (a) Zhao, W.; Song, Y.; Okamura, T.-a.; Fan, J.; Sun, W.-Y.; Ueyama, N. *Inorg. Chem.* **2005**, *44*, 3330−3336. (b) Li, W.; Barton, P. T.; Kiran, M. S. R. N.; Burwood, R. P.; Ramamurty, U.; Cheetham, A. K. *Chem.—Eur. J.* **2011**, *17*, 12429−12436. (c) Yang, Q.; Zhao, J.-P.; Hu, B.-W.; Zhang, X.-F.; Bu, X.-H. *Inorg. Chem.* **2010**, *49*, 3746−3751.

(9) (a) Hawxwell, S. M.; Espallargas, G. M.; Bradshaw, D.; Rosseinsky, M. J.; Prior, T. J.; Florence, A. J.; van de Streek, J.; Brammer, L. *Chem. Commun.* **2007**, 1532−1534. (b) Du, M.; Jiang, X.-J.; Zhao, X.-J. *Inorg. Chem.* **2007**, *46*, 3984−3995.

(10) (a) Chen, Q.; Guo, P.-C.; Zhao, S.-P.; Liu, J.-L.; Ren, X.-M. *CrystEngComm* **2013**, *15*, 1264−1270. (b) Zhan, C.-H.; Wang, F.; Kang, Y.; Zhang, J. *Inorg. Chem.* **2011**, *51*, 523−530. (c) Wang, J.-G.; Huang, C.-C.; Huang, X.-H.; Liu, D.-S. *Cryst. Growth Des.* **2008**, *8*, 795−798. (d) Jia, H.-P.; Li, W.; Ju, Z.-F.; Zhang, J. *Eur. J. Inorg. Chem.* **2006**, 4264−4270. (e) Marques, L. F.; dos Santos, M. V.; Ribeiro, S. J. L.; Castellano, E. E.; Machado, F. C. *Polyhedron* **2012**, *38*, 149−156. (f) Xu, J.; Cheng, J.; Su, W.; Hong, M. *Cryst. Growth Des.* **2011**, *11*, 2294−2301. (g) Zhang, Z.; Xiang, S.; Chen, Y.-S.; Ma, S.; Lee, Y.; Phely-Bobin, T.; Chen, B. *Inorg. Chem.* **2010**, *49*, 8444−8448. (h) Bon, V.; Senkovska, I.; Baburin, I. A.; Kaskel, S. *Cryst. Growth Des.* **2013**, *13*, 1231−1237.

(11) Earl, L. D.; Patrick, B. O.; Wolf, M. O. *CrystEngComm* **2012**, *14*, 5801−5808.

(12) Bureekaew, S.; Sato, H.; Matsuda, R.; Kubota, Y.; Hirose, R.; Kim, J.; Kato, K.; Takata, M.; Kitagawa, S. *Angew. Chem., Int. Ed.* **2010**, *49*, 7660−7664.

(13) Zhao, J.; Wang, X.-L.; Shi, X.; Yang, Q.-H.; Li, C. *Inorg. Chem.* **2011**, *50*, 3198−3205.

(14) Ni, Z.; Yassar, A.; Antoun, T.; Yaghi, O. M. *J. Am. Chem. Soc.* **2005**, *127*, 12752−12753.

(15) Bertrand, G. H. V.; Michaelis, V. K.; Ong, T.-C.; Griffin, R. G.; Dincă, M. *Proc. Natl. Acad. Sci. U.S.A.* **2013**, *110*, 4923−4928.

(16) (a) Gu, J.-M.; Kwon, T.-H.; Park, J.-H.; Huh, S. *Dalton Trans.* **2010**, *39*, 5608−5610. (b) Eddaoudi, M.; Kim, J.; Rosi, N.; Vodak, D.; Wachter, J.; O'Keeffe, M.; Yaghi, O. M. *Science* **2002**, *295*, 469−472.

(17) (a) Clot, O.; Wolf, M. O.; Patrick, B. O. *J. Am. Chem. Soc.* **2001**, *123*, 9963−9973. (b) Weinberger, D. A.; Higgins, T. B.; Mirkin, C. A.; Stern, C. L.; Liable-Sands, L. M.; Rheingold, A. L. *J. Am. Chem. Soc.* **2001**, *123*, 2503−2516. (c) Wong, W.-Y.; Choi, K.-H.; Lu, G.- L.; Lin, Z. *Organometallics* **2002**, *21*, 4475−4481.

(18) (a) Bai, S.-Q.; Yong, A. M.; Hu, J. J.; Young, D. J.; Zhang, X.; Zong, Y.; Xu, J.; Zuo, J.-L.; Hor, T. S. A. *CrystEngComm* **2012**, *14*, 961−971. (b) Schaate, A.; Schulte, M.; Wiebcke, M.; Godt, A.; Behrens, P. *Inorg. Chim. Acta* **2009**, *362*, 3600−3606. (c) Zhai, Q.-G.; Zeng, R.-R.; Li, S.-N.; Jiang, Y.-C.; Hu, M.-C. *CrystEngComm* **2013**, *15*, 965−976. (d) Cai, Y.; Zhang, Y.; Huang, Y.; Marder, S. R.; Walton, K. S. *Cryst. Growth Des.* **2012**, *12*, 3709−3713.

(19) Kahn, O. *Molecular Magnetism*; Wiley-VCH: New York, 1993.

(20) Alexandrov, E. V.; Blatov, V. A.; Kochetkov, A. V.; Proserpio, D. M. *CrystEngComm* **2011**, *13*, 3947−3958.

(21) *SAINT, Version 7.60A*; Bruker AXS Inc.: Madison, WI, 1997−2009.

(22) *SADABS*; Bruker AXS Inc.: Madison, WI, 2008.

(23) Altomare, A.; Burla, M. C.; Camalli, M.; Cascarano, G. L.; Giacovazzo, C.; Guagliardi, A.; Moliterni, A. G. G.; Polidori, G.; Spagna, R. *J. Appl. Crystallogr.* **1999**, *32*, 115−119.

(24) Sheldrick, G. M. *SHELXL-97, Programs for Crystal Structure Analysis, Release 97-2*; Institüt für Anorganische Chemie der Universität Göttingen: Göttingen, Germany, 1998.

(25) Farrugia, L. J. *J. Appl. Crystallogr.* **1999**, *32*, 837−838.

(26) van der Sluis, P.; Spek, A. L. *Acta Crystallogr., Sect. A* **1990**, *46*, 194−201.

(27) Naudin, É.; El Mehdi, N.; Soucy, C.; Breau, L.; Bélanger, D. *Chem. Mater.* **2001**, *13*, 634−642.

(28) Almutairi, A.; Tham, F. S.; Marsella, M. J. *Tetrahedron* **2004**, *60*, 7187−7190.

(29) Hulvey, Z.; Furman, J. D.; Turner, S. A.; Tang, M.; Cheetham, A. K. *Cryst. Growth Des.* **2010**, *10*, 2041−2043.

(30) Liu, X.-M.; Lin, T.; Huang, J.; Hao, X.-T.; Ong, K. S.; He, C. *Macromolecules* **2005**, *38*, 4157−4168.

(31) Van Bolhuis, F.; Wynberg, H.; Havinga, E. E.; Meijer, E. W.; Staring, E. G. *J. Synth. Met.* **1989**, *30*, 381−389.

(32) Geranmayeh, S.; Abbasi, A.; Skripkin, M. Y.; Badiei, A. *Polyhedron* **2012**, *45*, 204−212.

(33) Fisher, M. E. *Am. J. Phys* **1964**, *32*, 343−346.

(34) Menage, S.; Vitols, S. E.; Bergerat, P.; Codjovi, E.; Kahn, O.; Girerd, J. J.; Guillot, M.; Solans, X.; Calvet, T. *Inorg. Chem.* **1991**, *30*, 2666−2671.

(35) Carlin, R. L. *Magnetochemistry*; Springer: Berlin, 1986.

(36) Baca, S. G.; Malaestean, I. L.; Keene, T. D.; Adams, H.; Ward, M. D.; Hauser, J.; Neels, A.; Decurtins, S. *Inorg. Chem.* **2008**, *47*, 11108−11119.

(37) Dzyaloshinsky, I. *J. Phys. Chem. Solids* **1958**, *4*, 241−255.

(38) (a) Barrios, L.; Ribas, J.; Aromí, G.; Ribas-Ariño, J.; Gamez, P.; Roubeau, O.; Teat, S. J. *Inorg. Chem.* **2007**, *46*, 7154−7162. (b) Cheng, L.; Zhang, W.-X.; Ye, B.-H.; Lin, J.-B.; Chen, X.-M. *Eur. J. Inorg. Chem.* **2007**, 2668−2676. (c) Han, S.; Manson, J. L.; Kim, J.; Miller, J. S. *Inorg. Chem.* **2000**, *39*, 4182−4185.